1. CLIMATE AND ENVIRONMENTAL MODELLING

1.1 Ocean Modelling Activities

1.1.1 Sea Surface Height Studies

Altimeter data from the Topex/Poseidon (T/P) satellite for the years 1992 to present was procured from AVISO (Archive, Preview, Interpretation of Data of Oceanographic Satellites) France. The sea surface height (SSH) and sea surface anomaly data supplied by AVISO is on 0.25° latitude X 0.25° longitude at 10 day intervals. This altimeter data has been regridded into 1°latitude X 1°longitude and has been converted to *Netcdf* format for comparing with Modular Ocean Model (MOM) outputs.

SSH anomaly maps derived from the T/P altimeter data for a few typical months of the year 1996 are shown in Fig. 1.1.1.1. During January, a typical winter month, the SSH anomaly is positive along the Somali coast whereas negative SSH anomaly has been observed in November along the same coast and, also in the central Arabian sea region. In the equatorial Indian Ocean, positive SSH anomaly is observed during January, whereas, in a monsoon month like August, negative SSH anomaly is observed.

To study the seasonal variations of the Indian Ocean circulation features, model simulations using 6-hourly winds for the years 1995-1996 along with various surface fluxes were carried out; the wind data were from National Centre for Environment Prediction (NCEP), USA and Special Sensor Microwave Imager (SSM/I) data sets. The model outputs were analysed to study the SSH variations of the

Fig. 1.1.1.1. Monthly sea surface height anomaly maps derived from T/P altimeter data for the year 1996; (a) January, (b) May, (c) August and (d) November.
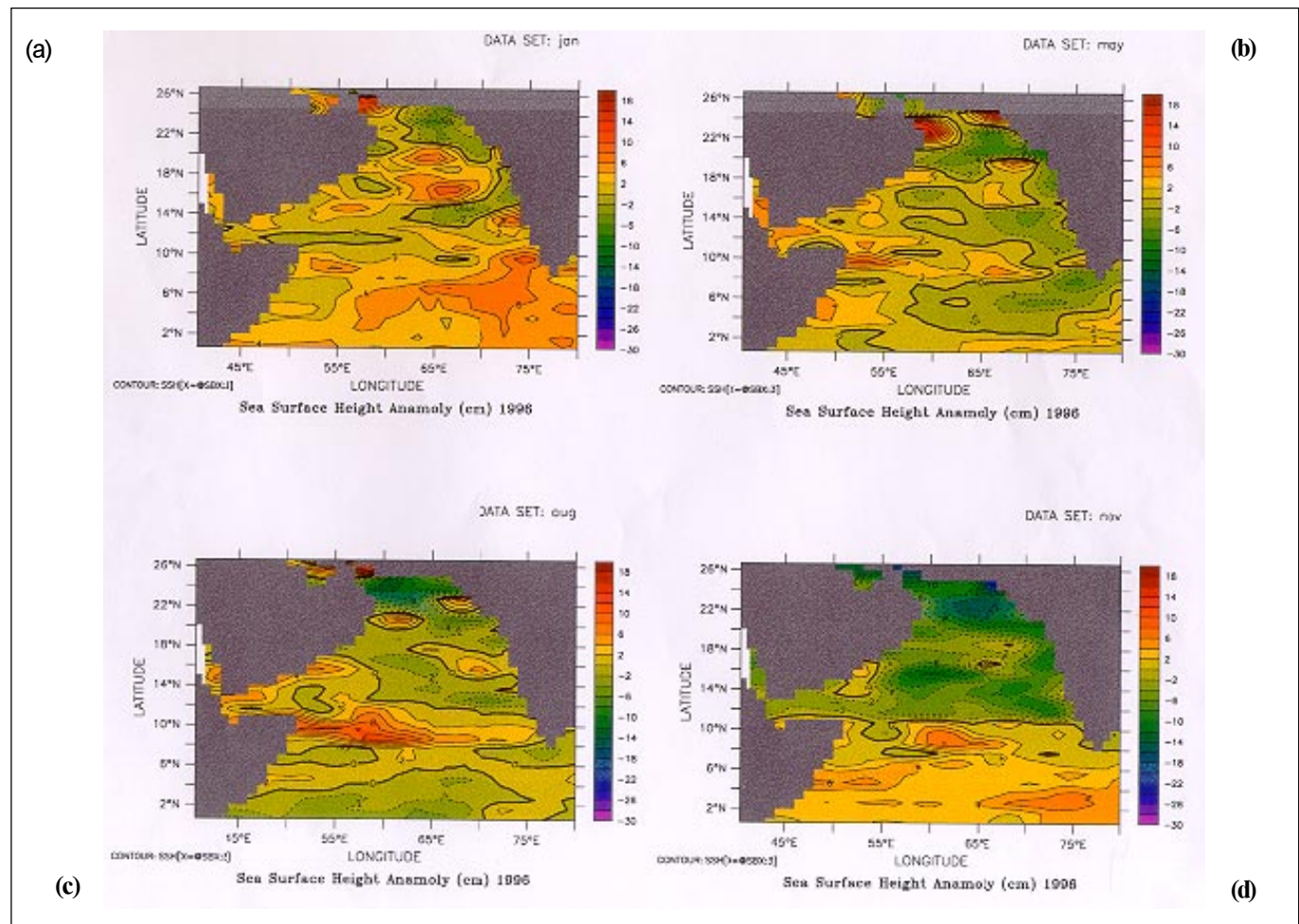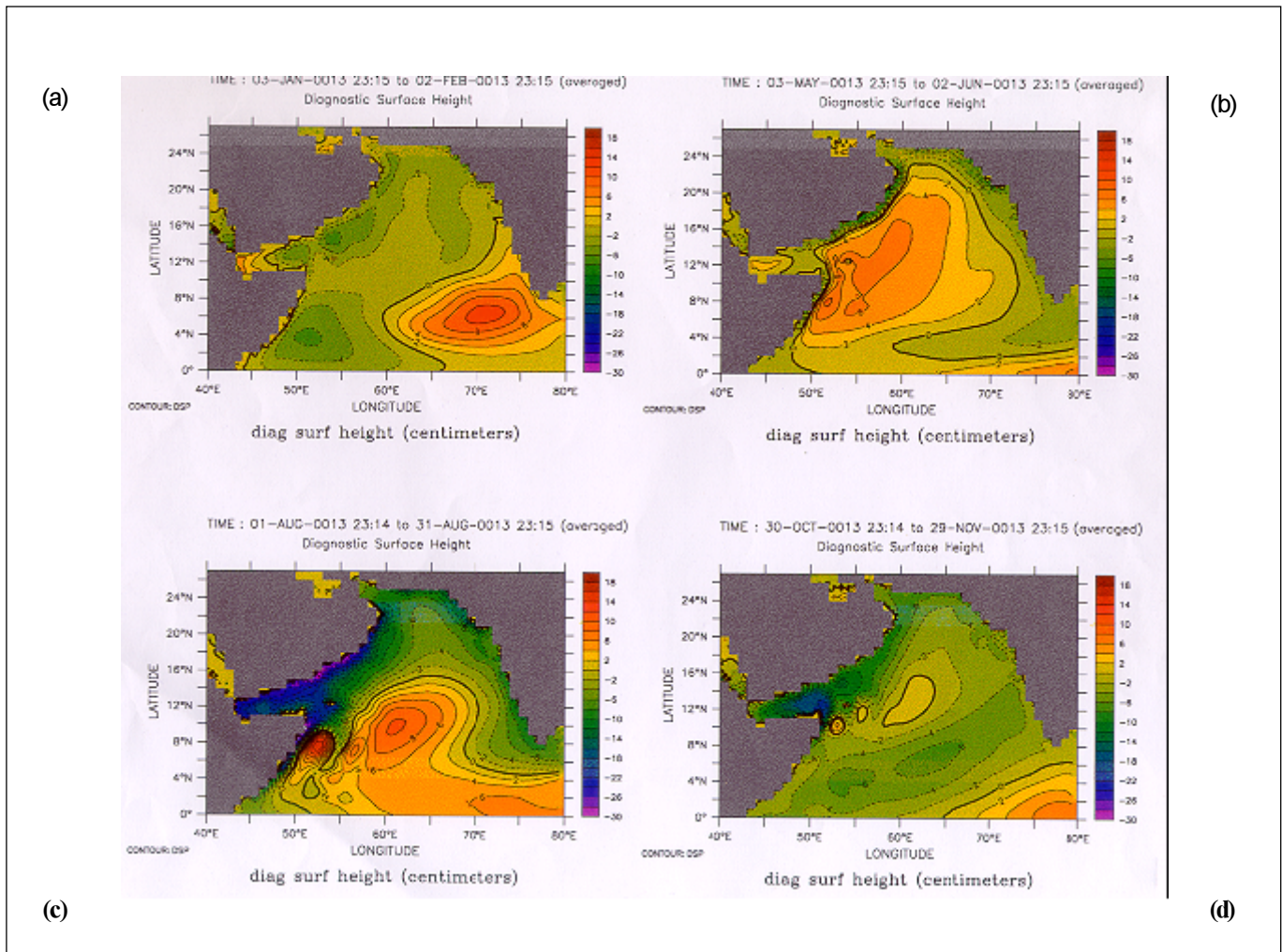
Fig. 1.1.1.2. Sea surface height from the climatologically forced model output for, (a) January, (b) May, (c) August and (d) November.

Arabian Sea and Bay of Bengal regions. Also, monthly SSH maps were generated from climatologically forced model outputs for a few typical months (January, May, August and November; Fig. 1.1.1.2). When these two are compared, the 6-hourly simulations (Figs. 1.1.1.3 and 1.1.1.4) show fine spatial and temporal structure compared to the climatologically forced runs as expected.

Figure 1.1.1.5 shows the zonally averaged (40-100 $^{\circ}$E) contour plot of SSH derived from the 6-hourly model simulations; the SSH variations show a clear pattern with alternate bands of positive and negative variations. Negative SSH variations are observed during November and December in both the years of 1995 and 1996. The model derived SSH maps are in good agreement with T/P derived zonal sea surface height variations.

(C Kalyani Devasena and P S Swathi)

1.1.2 Data Assimilation for Ocean Modelling Studies

As a part of the project, Indian Ocean Model and Dynamics (INDOMOD), for modelling and experimental forecasting of the Indian Ocean, the assimilation of altimeter data into MOM is in progress. Two different methods for data assimilation have been studied in this programme, the adjoint method and the nudging technique. The former guarantees full consistency with dynamics. The technique involves adjusting a model trajectory as closely as possible to the data by variation of control variables. To quantify the misfit of the model prediction, a cost function is introduced. This cost function is minimized by use of an iterative algorithm. Starting with a first guess, in each iteration step, an improved vector of the control variables is generated. The search direction is computed from the gradient of the cost function with respect to the control variables; the adjoint
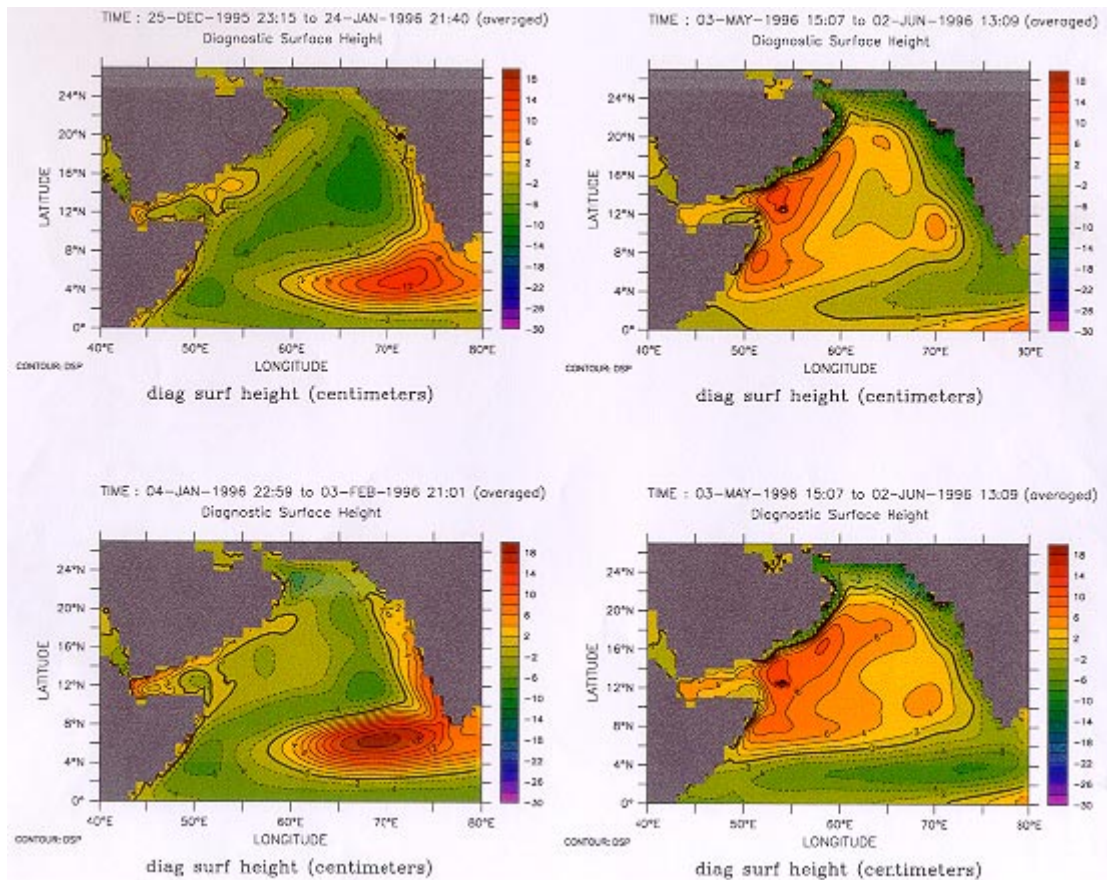
4

Fig. 1.1.1.3. Comparison of two different monthly sea surface height contour plots from the model using 6-hourly wind forcings; top panels use NCEP data for January (left) and May (right) while bottom panels use SSM/I data for 1996.

of the model computes this gradient vector. An automatic method of generating the adjoint of a model, called TAMC (Tangent Linear and Adjoint Model Compiler), has been procured and implemented at C-MMACS; this bypasses the time consuming direct coding of the adjoint of a model which can also be subject to errors. In data assimilation, the control variables typically determine the initial conditions or the forcings for the model.

We have completed a preliminary study of an idealised quasi-geostrophic (QG) model using the adjoint method. Efforts are underway to put realistic SSH into the QG model and its adjoint.

(K Sandeep, P S Swathi and C Kalyani Devasena)

1.1.3 Biogeochemistry of the Oceans

The oceanic uptake of carbon from the atmosphere and its sequestration in the oceans are of paramount importance

in the study of climatic change. In order to facilitate intercomparison between large scale simulations made by different groups, the Ocean Carbon-cycle Model Intercomparison Project (OCMIP) was established in the mid-1990s. Under the OCMIP protocols, the modelling groups were to adhere to a common set of procedures for biogeochemistry, which included a suite of abiotic and biotic simulations while being free to pick a circulation model of their choice.

1.1.4 Improvements to the Circulation Model

The OCMIP simulations showed some systematic deficiencies in the Princeton Ocean Biogeochemical Model (POBM) with the waters in the deep North Pacific being much too old. In order to correct these errors, the following changes were made in POBM: (1) European Centre for Medium Range Weather Forecasting (ECMWF) winds replaced Hellerman-Rosenstein winds, (2) the Drake
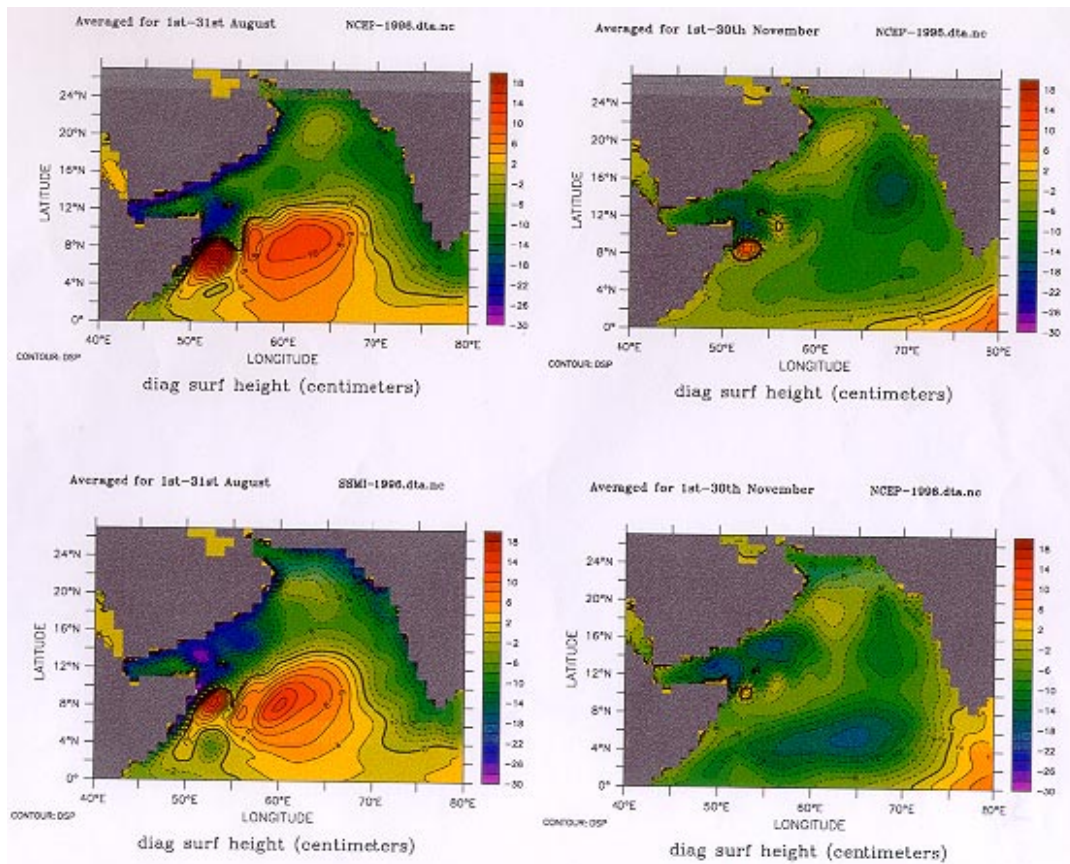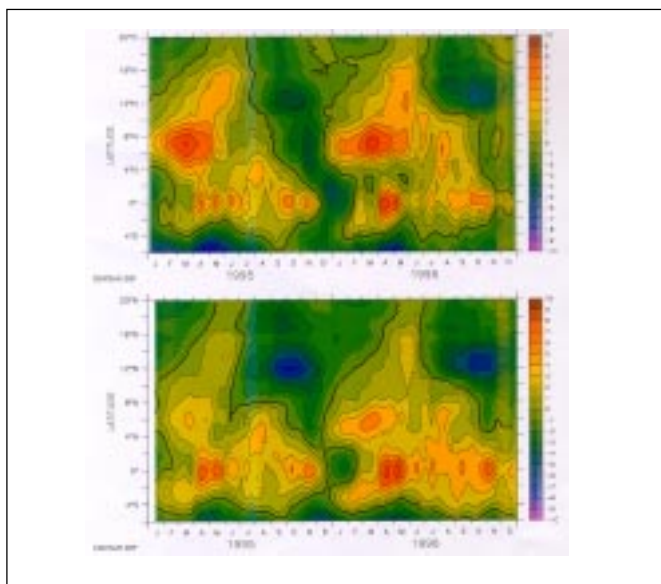
Fig. 1.1.1.4. Same as Fig. 1.1.1.3 but for August (left panels) and November (right panels).

Fig. 1.1.1.5. Time-Latitude plot of zonally averaged (40°-100°E) sea surface height from the model using 6-hourly wind forcings; (a) SSM/I and (b) NCEP, for the years 1995-1996.

Passage was narrowed by one grid box and, (3) Comprehensive Ocean Atmosphere Data Set (COADS) heat and salinity fluxes at the surface were replaced by diagnostic fluxes which were obtained during the run to equilibrium. These changes led to substantial improvement to the general circulation as can be seen in Fig. 1.1.4.1 where modelled and observed C14 are shown. Further improvements to the physical side of POBM (modification of the topography in the Sea of Japan and the incorporation of Levitus 98 surface data) are currently underway.

1.1.5 Improvements in Biogeochemistry

The biotic model of the OCMIP-II program was based on a simple diagnostic formulation of a restoring type of production of organic matter, conversion of a fixed fraction of this production into dissolved organic phosphate (DOP), which is advected and diffused in the General Circulation Model (GCM), and with the remaining production exported to depth and remineralised. This model left out the important
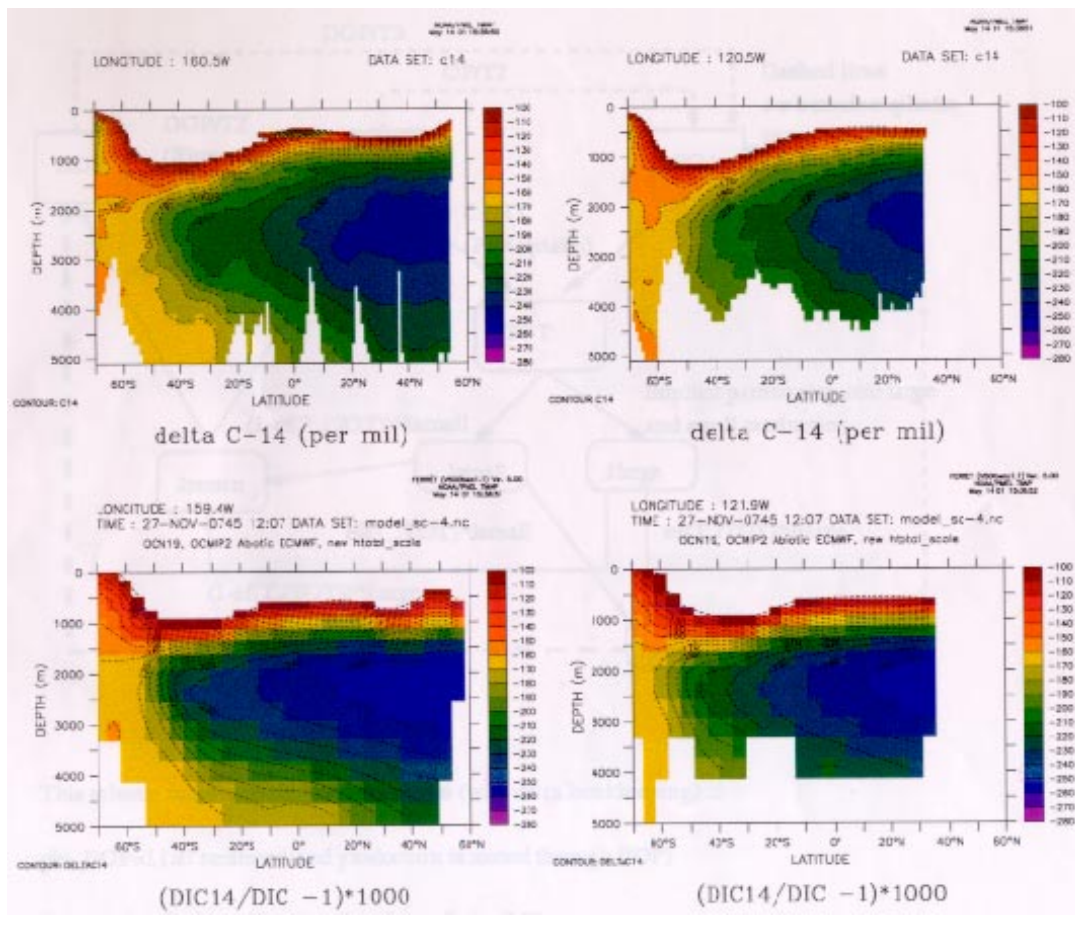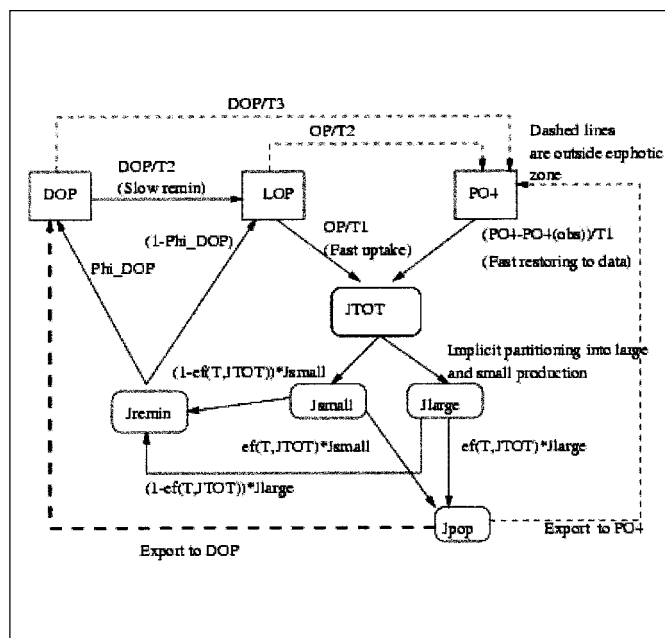
6

Fig. 1.1.4.1. Measured (top panels) and modelled (bottom panels) C14 along two WOCE sections.

Fig. 1.1.5.1. Schematic of the new biogeochemical model with implicit partitioning into small and large phytoplanktons.

distinction between small and large phytoplanktons which have very different behavior as far as export to depth is concerned. The large phytoplanktons are quite efficient in exporting biological production to depth. A new biogeochemistry model, simple in the sense that it avoids too many compartments, but still versatile in the sense that it allows an implicit partitioning of production into small and large size classes of phytoplanktons, has been developed (shown in Fig. 1.1.5.1) and incorporated into POBM. In the schematic, JTOT is the total primary production and the arrows leading from PO4 and LOP (labile organic phosphate) denote new and regenerated production respectively and, Jpop is the production which is exported to depth. The results from the new biogeochemical model (annual-averages) are shown in Fig. 1.1.5.2. Figure 1.1.5.3 shows the scatter-plot of the f-ratio vs. the e-ratio for different values of the parameter which controls the partitioning of the remineralisation between DOP and LOP; f-ratio is the ratio of new production to primary production and the e-ratio is the ratio of the export to depth to primary production. Notice that case (d) gives the tightest correlation between the two.
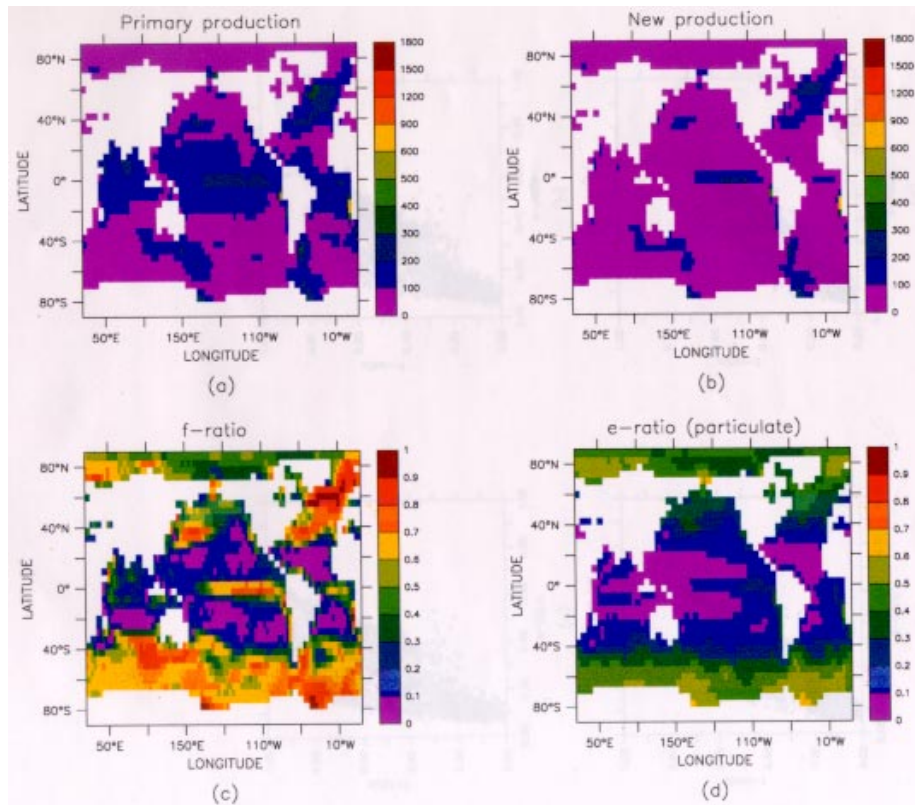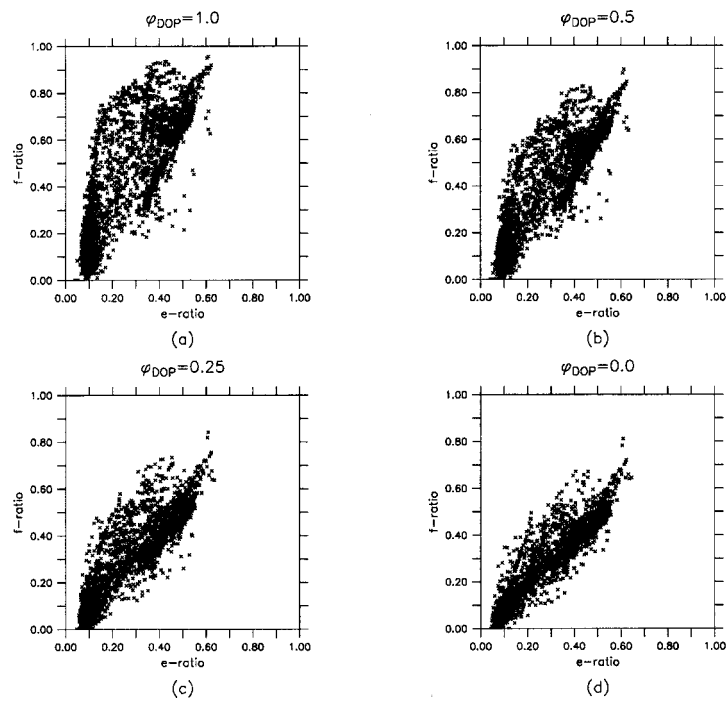
7

Fig. 1.1.5.2. Annual production and export to depth in the new model with phi_DOP = 0.0. The units for panels (a) and (b) are gC/sq.m/year: f-ratio is the ratio of new production to primary production and e-ratio is the ratio of the export to depth to primary production.

Fig. 1.1.5.3. Scatter-plot of f-ratio vs e-ratio.

8

A more comprehensive model involving several nutrients (nitrate, phosphate, silicate and iron) and explicit limitation of production by their availability is currently underway.

(Anand Gnanadesikan*, Jorge Sarmiento* and P S Swathi; *Princeton University)

1.1.6 Modelling and Experimental Forecasting of Biological Productivity

Several efforts have been initiated to obtain data on Ocean colour from recent satellites like SeaWiFS and IRS-P4. SeaWiFS was launched in 1997 (with a nominal mission duration of five years) and data acquisition commenced from September, 1997. SeaWiFS (Sea-viewing Wide Field-of-Satellite View Sensor) is a spectraradiometer, which measures radiance in specific bands of the visible light spectrum. The advantage of observing the Oceans with a space-based spectraradiometer is the global coverage that a satellite provides. The disadvantage is that interfering optical effects, like light scattering in the atmosphere, must be accounted for to derive measurement of the water-leaving radiance. Approximately 90% of the Ocean surface is scanned every two days by SeaWiFS and the data set consists of measurements of global and regional Ocean color data. When visible light from the Sun illuminates the Ocean surface, several optical effects like reflection, absorption etc. take place. The concentration and predominant identity of the substances and particles in the euphotic zone of the upper Ocean influences the apparent color of the Ocean, which can range from deep blue to varying shades of green and ruddy brown; light reflects off particulate matter suspended in the water, and absorption is primarily due to the photosynthetic pigments (Chlorophyll) present in phytoplankton. The operational parameters of the SeaWiFS mission were based on the heritage of the CZCS (Coastal Zone Color Scanner; the first instrument to collect scientific data on Ocean color, which operated from 1978 to 1986) mission and were designed to improve the acquisition and accuracy of Ocean color data for global and regional study of the Ocean biology and related physical oceanographic phenomena. The biogeochemical models can be validated using the satellite data to greater precisions because of the spatial and temporal coverage in the data. This is an important step towards data assimilation exercises in 3-D models.

SeaWiFS data is archived according to the standard remote sensing definitions of Level 1a, 2, and Level 3 data. Level-1a product is generated from Level-0 data files (raw radiance counts from all bands along with the spacecraft and instrument specifications) and so on. We have procured a few data sets in Level 1a and Level 2. We are in the process of acquiring Level 3 data sets for the Indian Ocean. All of the data products from SeaWiFS are stored in Hierarchical Data Format (HDF). HDF is a self-describing, platform independent format. HDF provides several different data models in the same file like Scientific Data Sets (SDS), 8-bit and 24-bit Raster Image Sets (RIS), Vdatas, Vgroups etc. which are used to store the data products. HDF library and utilities are available on a number of different machines and operating systems. Application interfaces can be used to manipulate the data sets in a file.

Fig. 1.1.6.1. Ocean colour data collected from SeaWiFS for two stations in Arabian Sea from 16 September 1997 to 31 December 1997; (a) station at 16^0 N, 65^0 E and, (b) station at 20^0 N, 70^0 E.
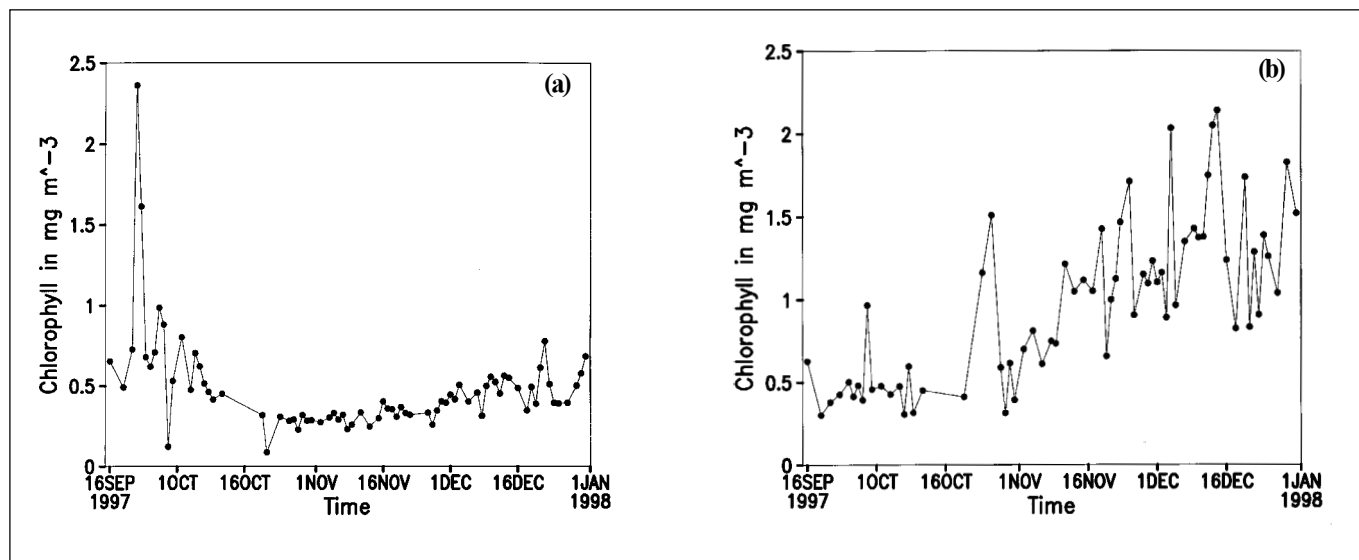
There are two distinct types of SeaWiFS data, LAC and GAC. GAC data is the global SeaWiFS data product, obtained at 4 km resolution over most of the world's oceans and LAC data is available at 1 km resolution for specific regions. A software for the specific purpose of analysing and processing SeaWiFS HDF data products, SEADAS, was downloaded with the embedded Interactive Descriptive Language (IDL) runtime library and is being installed on SGI platform. Figure 1.1.6.1 shows the data on chlorophyll obtained from SeaWiFS data at two locations in the Arabian Sea. Several other software packages which are used for reading and manipulating HDF data products are being studied to get an understanding of the different levels of SeaWiFS data.

(K Anjali, M K Sharada and K S Yajnik)

1.1.7 Sea Level Variations

Earlier work on sea level variations was focused on the time series analysis of sea level variations at different coastal sites in the Indian Ocean region. Both linear stochastic time series and nonlinear time series analyses of data had been carried out.

As a continuation of this study, a multivariate analysis of sea level data along with other oceanic variables such as meridional and zonal velocities, salinity and sea surface temperature was carried out. All the above were extracted from a Modular Ocean Model (MOM) simulation of the global Ocean. The data was representative of different geographical regions and the analysis was repeated for each region. In other words, the data is grouped according to different regions and the relationship of these variables are being studied within the group and between the groups. Preliminary results indicate that it would be possible to reduce the number of degrees of freedom in order to facilitate inversion and assimilation of sea level data in Ocean models.

(N K Indira)

1.2 Atmosphere Modelling Activities

1.2.1 High Resolution Monsoon Simulation: Evaluation with Two Contrasting Years

Simulation and forecasting of monsoon rainfall, especially with high spatial resolution, is a formidable challenge. Most General Circulation Models (GCMs) can claim only moderate skill, at best, in simulating monsoon rainfall,

especially its variabilities. One of the crucial steps for progress in this aspect is the identification of parameters, processes and procedures that have significant impact on the precipitation forecast.

In a complex system like a GCM, numerous factors influence the quality of simulation, not all of which are easily identified. Among the factors that are known to play critical roles, horizontal resolution (HR) of the model is certainly one. Although enhanced HR improves simulation in general, the improvement is not uniform for all aspects of simulation and, also, saturation effects have been notified. It may be emphasized that the question of the effect of HR in a GCM is a complex one, since, in such a situation, a clear separation between numerics (such as resolution) and physics (such as convective heating) no longer exists. The change of HR can dramatically change the nature of scale interaction and the dynamical quantities leading, in particular, to redistribution of convergence and associated precipitation centers. This issue becomes more complex when the horizontal resolution is non-uniform; a variable resolution (VR) simulation is, in general, distinct from a (comparable) high resolution simulation.

Because of the close interplay between numerics and physics, a well-chosen grid can, through a variety of mechanisms, significantly alter (and improve) the simulation. We have explored this methodology with a variable resolution GCM for simulating the Indian summer monsoon. The summer monsoon is a large-scale system; high resolution is therefore expected to improve simulation both over the monsoon region and away from it. This strategy has been evaluated by considering two widely

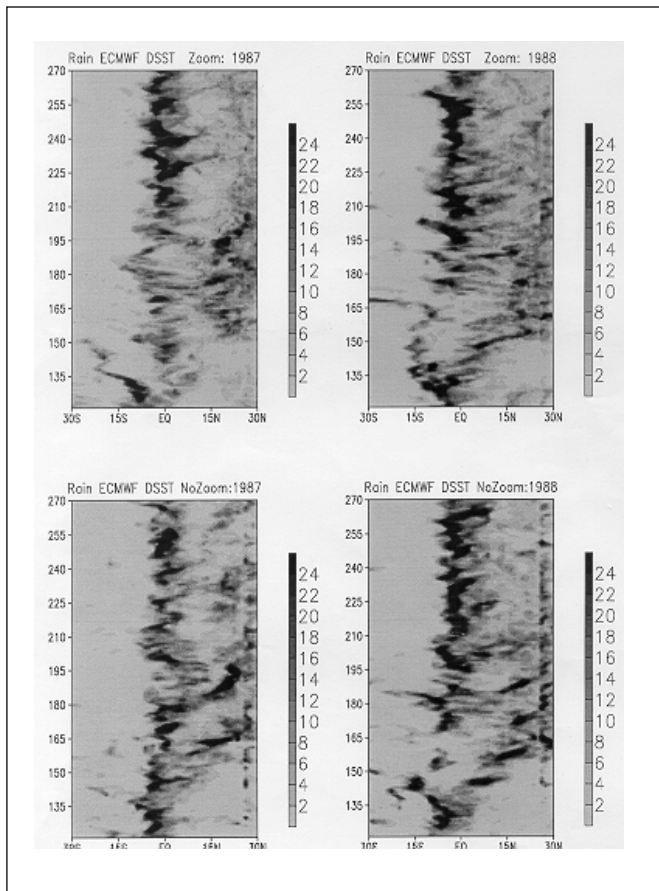**Fig. 1.2.1.1.** Zoom grid with zoom center at (75^0 E, 15^0 N).
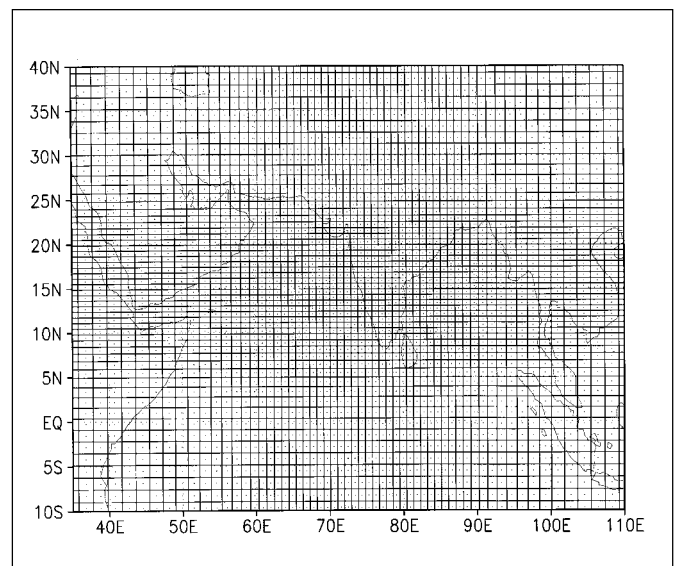
Fig. 1.2.1.2. Latitude-time structure of precipitation field for ECMWF daily SST fields for zoom grid (top panels) and uniform grid (bottom panels) for 1987 (left panels) and 1988 (right panels). The x-axis shows latitude in degrees while the y-axis shows time in days starting from 120 (May 1). The precipitation fields are averaged over 88⁰E and 90⁰E; the scale of precipitation in mm/day is shown alongside.

upon the source or the method used to generate these fields.

The initial states were prescribed from European Centre for Medium Range Weather Forecasts (ECMWF) analyses, interpolated to the model grid. A large number of experiments were carried out for each of the two years, both for UG and zoom grid (ZG). A large amount of diagnostics is possible with the simulations from a GCM. The focus of the present work, however, is on precipitation field.

To contrast the UG and ZG simulations, the latitude-time (*y-t*) structures of rainfall from the two simulations are shown in Fig. 1.2.1.2. For 1987, it can be seen that a major southward shift of the precipitation belt occurred during this phase (day 155 to day 175) with very little precipitation in the latitudinal belt 12-30⁰N. The short duration of the rainfall season for 1987 is very clear from the *y-t* diagram for the ZG; there is very little rain in the latitudinal belt 10-30⁰N beyond day 210 (July 30). In contrast, the UG simulation for 1987 (bottom left panel) shows a much more prolonged rainfall activity. On the other hand, for 1988 (right panels), the y-t diagram shows a shorter (and weaker) monsoon for UG than for ZG; the role of the zoom seems to be to almost diametrically reverse the structures for 1987 and 1988. A major difference in the progress of the two monsoons can be seen from the *y-t* diagram of precipitation. The monsoon of 1988 is characterized by a strong northward shift of the precipitation belt in the early stages of the monsoon (beginning of June). In contrast, in spite of its strong initial phase, the major precipitation belt in 1987 stayed over the equator, and shifted southward subsequently.

contrasting monsoon years, 1987 and 1988; the contrast years provide a challenging testing ground for a GCM. The year 1988 marked a sharp transition from a series of poor monsoon years to an excess monsoon year. Another advantage is that these years have been employed by other workers as well, thus providing opportunity for comparisons.

We have adopted the version LMDZ3.2 of the AGCM developed at Laboratory for Dynamic Meteorology (LMD); this can support a zoom (higher horizontal resolution) around a given point. Figure 1.2.1.1 shows a part of the model grid with the zoom. The highest resolution (near the centre of the zoom) is about 0.8 x 0.6 degrees (longitude x latitude), which merges uniformly with a resolution of 2 x 2 degrees away from the zoom. In the context of the saturation effect mentioned earlier with respect to increased HR, the uniform grid (UG) resolution is near optimum. In all the experiments, the sea surface temperature (SST) field varies daily. However, this daily variation can be different depending

To bring out, more clearly, the contrast of the two simulations (1987 and 1988), we show in Fig. 1.2.1.3 category rainfall maps for the four months; here -1, 0 and 1 correspond to low (< 5 mm/day), medium (5-10 mm/day) and high (>10 mm/day) rainfall. While the simulations in Fig. 1.2.1.2 were generated with 30th December initial conditions of the preceeding year, the simulations in Fig. 1.2.1.3 were generated with 30th May initial conditions for the corresponding year. Both the simulations are for ZG with daily SST from ECMWF dataset. The simulated precipitation fields are different for each month, with a clear deficit for 1987 over 1988.

VR GCMs offer a less explored but promising avenue for generating high resolution forecasts of monsoon rainfall. A detailed investigation to evaluate hindcast skills of the method at different scales is in progress.

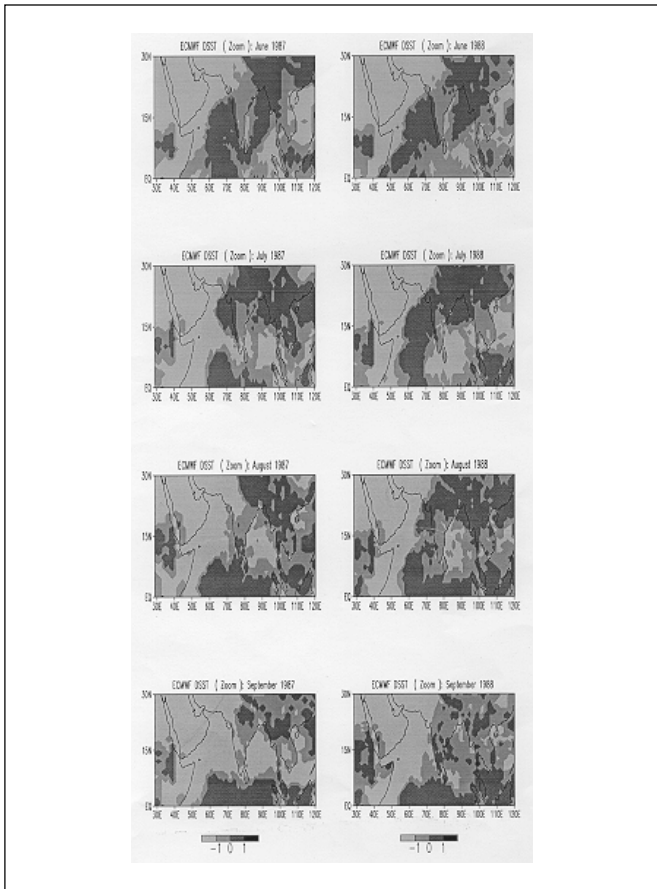*(P Goswami and Levan Phu*; *LMD, Paris)*

Fig. 1.2.1.3. Category maps of rainfall for the two contrasting years 1987 (left panels) and 1988 (right panels) for the four monsoon months. Here −1,0 and 1 imply <5 mm/day, 5-10 mm/day and >10 mm/day respectively.

1.2.2 Diagnostic Application of 4-Dimensional Variational Assimilation

Assimilation of data is a critical component in operational forecasting of atmosphere and Ocean. 4-dimensional variational assimilation (4D-VAR) has emerged as a powerful tool in this area. Currently, 4D-VAR is operational at ECMWF since November, 1997, and at Meteo-France since June, 2000, with positive impact on the forecasts. The scope of applications of 4D-VAR, however, can be much larger. In particular, it can serve as a powerful diagnostic tool. At the same time, there remain crucial issues like objective and quantitative evaluation of the process of 4D-VAR and inclusion of model errors (ME). We briefly describe here our work on the identification of ME in the assimilating model.

Conventional 4D-VAR effectively reduces a constrained variational problem for the state vector over the entire assimilation interval (AI) to an unconstrained problem for the lower dimensional *reduced control variables*, for example the initial conditions. An implicit assumption in this conversion from constrained to unconstrained variational problem is that the constraint is exact. There have been a number of suggestions for ways to introduce the ME as a weak constraint. One possibility is to introduce extra terms in the model equations to represent the *misfit* of the model. The minimization is then carried out with an augmented set of control variables which includes these additional forcings.

As a part of the identification and assessment of ME in 4D-VAR, we have investigated the nature of the adjoint solution; the adjoint equation is used to compute the gradient of the objective function in 4D-VAR, The adjoint solution is a linear transform, through the adjoint equations, of the observations minus the minimizing solution. Any statistically significant feature of the adjoint solution is a signature of a statistical property of the modelling and/or observational error. At the minimum, the adjoint solution consists of the Lagrange multipliers associated with the constraints expressed by the model equations. As such, it indicates how the latter should be modified in such a way that the model solution fits the observations more closely.

In general, we expect the norm of the adjoint solution (NAS), considered as a function of time, which is zero at both ends of the AI, to attain a maximum at a point inside the AI. However, the characteristics of this evolution, the amplitude of the maximum, as well as other properties (such as the time of attaining the maximum) may vary from one case to another, and may carry the signature of ME. We have examined some of these issues using a global atmospheric model of intermediate complexity.

The atmospheric model we adopted is the three-layer quasigestrophic model developed by Marshall and Molteni. In the present case, we have considered a version of the model with three vertical levels at 200, 500 and 800 mb, and a truncation number 21 (T-21); the initial conditions were obtained from ECMWF Reanalyses for the winter of 1986 (01.01.1984, 0 GMT). To begin with, we generate a reality, in this case with the fully nonlinear model. The observations are then synthesized by adding a white noise observational error (OE) to the reality. The amplitude (rms) of the OE is given in such a way as to be about 10% of the standard deviation of the reality field. The ME in the present case was introduced by considering a reality generated by modifying the empirical forcings in the model.

Experiments were then carried out for different values of ME. Here we consider three cases: zero ME (ZME), small ME (SME) and large ME (LME). For each value of the ME, assimilation experiments were then carried out by varying the AI from 12 hours to 48 hours, in steps of 6 hours.

Table 1.2.2.1 summarizes the assimilation experiments in terms of the quantities defined below.

$$\delta = \frac{<X_{real} - X_{obs}>}{<X_{real}>}\text{x100},$$

$$J_0 = \frac{2J_{min}}{p} \qquad \epsilon_g = \frac{\nabla J_f}{\nabla J_i}$$

$$\eta_1 = \frac{<X_{obs} - X_{opt}>}{<X_{obs}>}\text{x100},$$

$$\eta_{ic} = \frac{<X_{real}(0) - X_{opt}(0)>}{<X_{real}(0)>}\text{x100},$$

Here J_{min} is the value of the objective function at the minimum and ∇J_f and ∇J_i are the final and the initial values

Sl.No.	Expt		Model Error		Minimization		Assessment		
	Name	δ	ΔF	Div	J_0	ϵ_g(x10^{-5})	η_{ic}	η_1	Aadj
1	ZME OE	9	0	0	0.97	1.9	3.5	10.6	4.2
2	SME-TIF	9	1	4	1.00	1.7	3.6	10.7	4.2
3	LME-TIF	9	5	17	1.02	3.5	4.5	10.8	4.4
4	SME-TDF	9	1	4	1.00	2.1	3.6	10.7	4.2
5	LME-TDF	9	5	17	0.98	0.43	8.3	10.8	3.3

Sl.No.	Expt		Model Error		Minimization		Assessment		
	Name	δ	ΔF	Div	J_0	ϵ_g(x10^{-5})	η_{ic}	η_1	Aadj
1	ZME OE	9	0	0	1.10	4.7	2.2	10.6	9.2
2	SME-TIF	9	1	4	1.12	10.1	4.5	10.7	10.4
3	LME-TIF	9	5	17	1.23	4.8	8.8	10.8	22.6
4	SME-TDF	9	1	4	1.12	1.5	2.4	10.7	12.5
5	LME-TDF	9	5	17	1.11	5.6	2.2	10.8	9.2

Table 1.2.2.1. Summary of the assimilation experiments; top table is for an assimilation interval of 12 hours and bottom table for 48 hours.

of the gradient function, respectively. It can be seen that the quantity ϵ_g is 10^{-5} in all the cases, although it increases with increasing AI, and with increasing ME for the same AI. Similarly, the quantity η_1 is 10.6, with the smallest value for the longest AI, as expected. Although these values of

Fig. 1.2.2.1. The norm of the RMMS for the quasi-geostrophic model for three values of model error: zero (solid curve), weak (dashed curve) and strong (dash-dot curve) for different assimilation intervals as indicated.
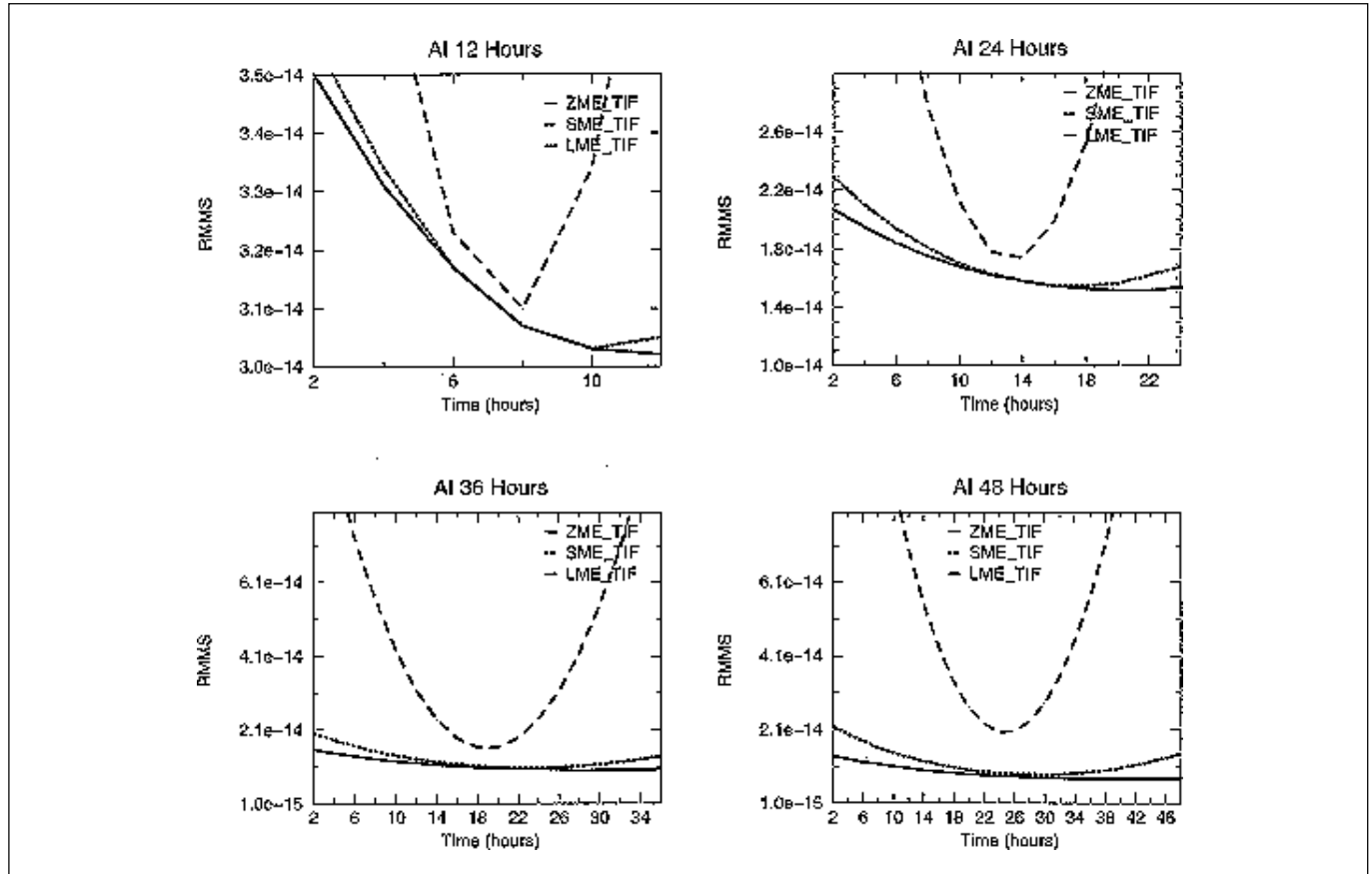
Fig. 1.2.2.2. The norm of the adjoint solution for the quasi-geostrophic model for three values of model error: zero (solid curve), weak (dashed curve) and strong (dash-dot curve) for different assimilation intervals as indicated.
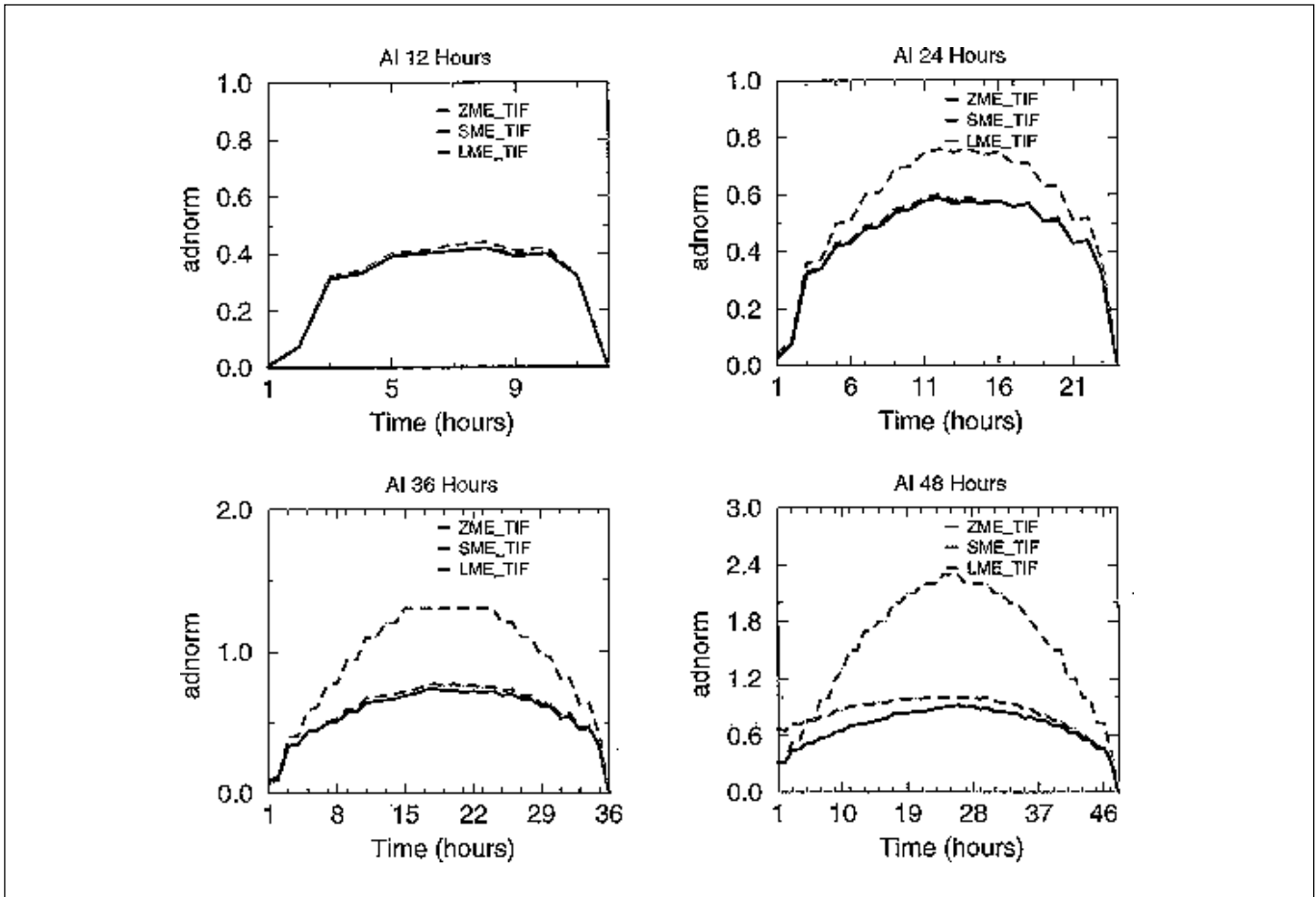
$\in_g$ and η_1 may seem to indicate an acceptable performance of the assimilation procedure, it should be noted that the quantity J_o is considerably different from its theoretical value (1.0 ± 0.01) for the case of strong ME and AI of 48 hours. This indicates need for multiple checks and *a posteriori* validation of the assimilation procedure.

It is possible to carry out checks with other quantities in the (ideal) case where the underlying reality is available. One such quantity is the Reality-Minus-Minimizing-Solution (RMMS). Considered as a function of time, the RMMS must exhibit a negative concavity in the AI. Figure 1.2.2.1 shows the norm of RMMS for the three cases of ME and for two AI, as indicated. In all the cases, the curves conform to the expected behaviour.

As we have mentioned earlier, the NAS is a potential diagnostic tool. Figure 1.2.2.2 presents the NAS as a function of time for the three cases of ME (for TIF, time-independent forcing perturbation) and for four values of AI. The most important result is that, while in the absence of

ME (solid line), the adjoint solution shows no appreciable change with the change of AI, there is a significant change (AI 12 hours and AI 48 hours) for the strong ME case. Since the adjoint solution is readily available during a 4D-VAR, the above result implies that it can be used to examine the presence of ME in the assimilating system.

(P Goswami and O Talagrand*; *LMD, Paris)

1.2.3 Neural Network Forecast (Cognitive Forecast) of Rainfall

The generalized neural network, termed cognitive network (CN), designed and developed at C-MMACS, has been used to generate long-range (one year or more) forecasts of all-India summer monsoon rainfall (ISMR), on an experimental basis, since 1996. These forecasts, generated well ahead of the seasons, have shown considerable skill in the

14

experiments conducted so far. In particular, the forecast of ISMR for the year 2000 had been generated and published two seasons in advance as 791 mm with an error bar of 30 mm, which is about 89% of a mean of 887 mm; the observed value was 92%. In Table 1.2.3.1, we compare the CN forecasts for the past six years with the observed values. Following our philosophy of generating experimental forecasts for objective evaluation of our methodology, we record here our experimental forecast of ISMR as 874 mm and 904 mm for 2001 and 2002 respectively; The much larger range of CN forecasts can be used to complement and supplement shorter range operational forecasts.

(P Goswami)

Table 1.2.3.1. Rainfall as percentage of mean; mean monsoon rainfall adopted in this table is 887 mm. (* indicates forecasts made 2 years in advance).

Year	CN Forecast	Observation
1995	98	100
1996	95*	103
1997	98	102
1998	107*	106
1999	98	96
2000	91*	92